MOLECULAR PHYSICS REPORTS **40** (2004) 137-143

GROWTH AND COERCIVITY BEHAVIOUR IN Fe/Zr MULTILAYERS

L. SMARDZ[1] AND K. SMARDZ[2]

[1]*Institute of Molecular Physics, Polish Academy of Sciences*
Smoluchowskiego 17, 60-179 Poznań, Poland

[2]*Institute of Materials Sciences and Engineering, Poznań University of Technology*
M. Curie 5 Sq., Poznań, Poland

Abstract: Fe/Zr multilayers with either wedged Fe or wedged Zr sublayers were prepared at room temperature using UHV magnetron sputtering. The planar growth of the Fe and Zr layers was confirmed *in-situ* by X-ray photoelectron spectroscopy. Iron sublayers grow on sufficiently thick zirconium ($d_{Zr} > 0.7$ nm) sublayers in the soft magnetic nanocrystalline phase up to a critical thickness $d_{crit} \sim 2.3$ nm. For a thickness greater than d_{crit}, the Fe sublayers undergo a structural transition to the polycrystalline phase with much higher coercivity.

1. INTRODUCTION

Metallic multilayers (MLs) composed of alternating sublayers of ferromagnetic and non-magnetic metals exhibit interesting magnetic properties which can be tailored by varying the composition and thickness of the sublayers. For potential application, the coercivity of multi-layered structures is an important parameter. For instance, such a structure for magnetic head application should be magnetically soft exhibiting high saturation magnetisation [1].

In the previous papers [2, 3], we showed that below the critical Co thickness (d_{crit}), the Co/Zr ($d_{crit} \sim 2.8$ nm) [2] and Co/Ti ($d_{crit} \sim 3$ nm) [3] MLs with constant-thickness sublayers are magnetically soft and exhibit a saturation magnetisation higher than that observed in conventional soft magnetic films. It has been found that up to d_{crit} Co sublayers grow in the soft magnetic nanocrystalline structure [4]. Above d_{crit}, Co sublayers grow in the polycrystalline structure with the average Co grain size greater than the magnetic exchange length. Very similar magnetic domains transition associated with a structural transition we have also observed earlier in wedged Fe/Zr multilayers [5]. Results reported in Ref. [6] also showed that the polycrystalline Co sublayers ($d_{Co} = 17$ nm) are very weakly exchange coupled or decoupled for Ti (Zr) spacer thickness equal to about 2.7 (3.2) nm. The small decoupling Ti (Zr) thickness was explained by spontaneous formation of a quasi-amorphous structure of the paramagnetic spacer during the deposition process [6].

On the other hand, it is well known that suitable annealing of the Fe/Zr MLs leads to the formation of an amorphous phase due to a solid state reaction [7-9]. Therefore the spontaneous formation of a quasi-amorphous or nanocrystalline interface Fe-Zr alloy layer is very likely to proceed during deposition of the Fe/Zr/Fe trilayer and especially Fe/Zr MLs. This is also consistent with the results of X-ray diffraction and magnetisation studies of Fe/Zr MLs reported in Ref. [8-9].

In this paper we study the influence of microstructure on the coercivity and in-plane uniaxial anisotropy. We also report on the stability range of the polycrystalline and soft magnetic nanocrystalline Fe phase as a function of Zr and Fe sublayer thicknesses. The deposition of the Fe and Zr sublayers in a linear or step-like wedge form removes the uncertainty associated with preparation conditions and sublayer thickness reproducibility. The magnetic properties (anisotropy and coercivity) of the wedged samples could be studied by scanning the light beam of a Kerr hysteresograph across the wedge.

2. EXPERIMENTAL PROCEDURE

Fe/Zr MLs were prepared onto glass substrates at 285 K using computer-controlled ultra high vacuum (UHV) magnetron co-sputtering. Fe and Zr targets were sputtered using DC and RF modes, respectively. The base pressure before the deposition process was lower than 5×10^{10} mbar. The chemical composition and the cleanness of all layers was checked *in-situ*, immediately after deposition, transferring the samples to an UHV (4×10^{11} mbar) analysis chamber equipped with X-ray photoelectron spectroscopy (XPS). The XPS spectra were measured with Al-K_α radiation at 1486.6 eV at room temperature using a SPECS EA 10 PLUS energy spectrometer. All emission spectra were measured immediately after *in-situ* sample transfer in a vacuum of 8×10^{11} mbar.

The deposition rates of Fe and Zr were individually checked by a quartz thickness monitors. The thicknesses of individual sublayers were mainly controlled by varying their deposition times. The number of repetitions was increased with decreasing Fe and Zr sublayer thicknesses, so as to keep the total thickness of the samples equal to about 50 nm and 500 nm for the magnetooptical measurements and X-ray diffraction studies, respectively. The Fe/Zr MLs were prepared with either wedged Fe or wedged Zr sublayers. Wedge-shaped Fe or Zr sublayers with a slope of 0.05-0.125 nm/mm were grown by moving a shutter linearly or stepwise in front of the substrate during deposition. Typical sputtering conditions used during the deposition of Fe/Zr MLs were collected in Table 1.

Table 1. Typical sputtering conditions used for deposition of Fe/Zr multilayers

Parameter	Unit	Fe	Zr
Rest gas pressure	mbar	5×10^{10}	
Argon partial pressure	mbar	5×10^{4}	
Argon purity	%	99.9998	
Target diameter	mm	51.5	
Target purity	%	99.997	99.99
Distance between substrate and target	mm	220	
Sputtering method		Magnetron RF	Magnetron DC
Sputtering power	W	45-60	60
Deposition rate	nm/s	0.05-0.08	0.04

Substrate temperature	K	285

The structure of the samples with step-like wedge form (areas with constant-thickness Fe and Zr sublayers) was examined *ex-situ* by standard θ-2θ X-ray diffraction with Cu-K_α radiation. The modulation wavelength was determined from the spacing between satellite peaks in the low-angle X-ray diffraction patterns. The results were consistent with the values obtained from total thickness divided by the number of repetitions. The thicknesses of individual Fe and Zr sublayers were also determined using X-ray fluorescence analysis (XRF). The magnetic characterisation of the wedged Fe/Zr MLs was carried out using the magnetooptical Kerr effect at room temperature. The coercive (H_c) and uniaxial anisotropy fields (H_k) were determined from the in-plane hysteresis loop measurements at room temperature.

3. RESULTS AND DISCUSSION

The composition modulation of the Fe/Zr MLs was confirmed in the low-angle X-ray diffraction measurements. We have observed from two to five satellite peaks for the MLs with the thinner and the thicker sublayers, respectively. The wavelengths of modulation calculated from these peaks were in agreement with the values determined from XRF measurements. In Fig. 1 we show an example of the low-angle X-ray diffraction pattern for 2 nm – Fe / 2 nm – Zr (Fig. 1a) and 4 nm – Fe / 4 nm – Zr (Fig. 1b) MLs. The intense satellite peaks reveal good artificial periodicity of the multilayered samples.

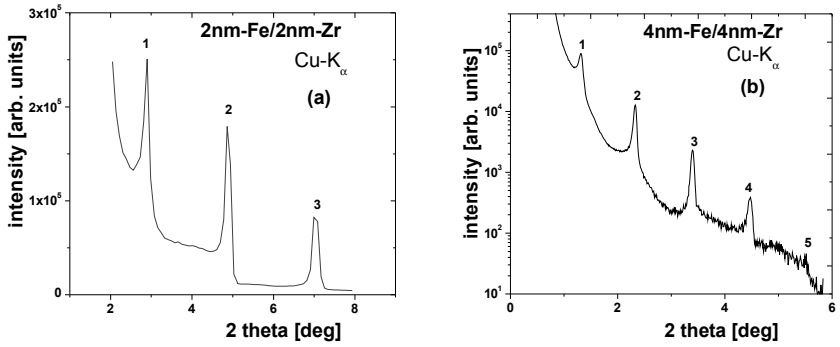

Fig. 1. Low-angle X-ray diffraction pattern (Cu-K_α) for the 2 nm – Fe / 2 nm – Zr (a) and 4 nm – Fe / 4 nm – Zr (b) multilayers

For Fe and Zr sublayer thickness equal to about 2 nm the peak observed in the high-angle X-ray diffraction pattern disappears. This is probably due to nanocrystalline or amorphous structure of the sublayers. The Fe/Zr MLs with sublayer thicknesses greater than ~3 nm showed the average Fe and Zr crystallite sizes in direction perpendicular to the substrates, as determined from the Scherrer equation, are comparable to their respective sublayer thicknesses. The absence of the Fe and Zr reflections for $d_{Fe} < \sim 2.3$ nm could be explained by nanocrystalline grow of the sublayers (average grain size $D << 10$ nm) similar to that observed

earlier for the Co sublayers in Co/Ti and Co/Zr MLs [2-4]. In the XPS experiment we have also studied the Fe layer growth on a 10 nm Zr underlayer and the Zr layer growth on

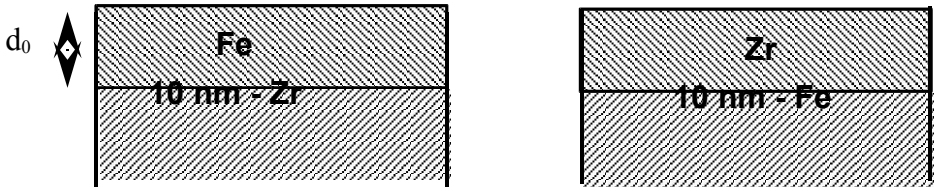

Fig. 2. Schematic description of the Fe (Zr) growth on 10 nm – Zr (10 nm – Fe)

10 nm – Fe underlayer. Schematic description of the Fe (Zr) overlayer growth on 10 nm – Zr (10 nm – Fe) is shown in Fig. 2. The freshly deposited 10 nm – Zr / d_0 – Fe or 10 nm Fe / d_0 Zr bilayer was *in-situ* transferred from the preparation chamber (5×10^{10} mbar base pressure) to the analysis chamber (4×10^{11} mbar base pressure), where the XPS Fe-2$p_{3/2}$ and Zr-3$d_{5/2}$ core level spectra were immediately measured in vacuum of 8×10^{11} mbar. Then the bilayer was transferred back to the preparation chamber and the deposition process of the overlayer was continued. The above procedure (overlayer deposition and XPS core level measurements) was repeated until the Fe-2$p_{3/2}$ and Zr-3$d_{5/2}$ integral intensities were saturated. Practically no trace of oxygen (or any other contaminations) adsorption or surface oxide formation was detected during the transfer operation or XPS measurements (~10 min). In Fig. 3 we show XPS spectrum of 20 nm – Fe overlayer deposited on 10 nm – Zr underlayer. As described above, no XPS signal is observed from potential contamination atoms like O:1*s* and C:1*s* (see Fig. 3). Furthermore, due to small roughness of 10 nm – Zr underlayer and 20 nm – Fe overlayer we have also observed no XPS signal from the bottom Zr layer.

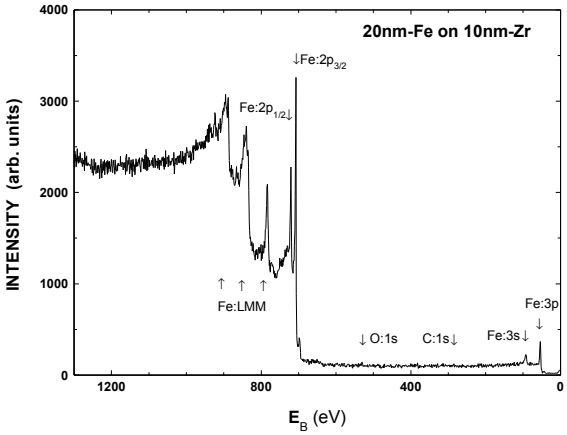

Fig. 3. XPS spectrum of 20 nm – Fe overlayer deposited on 10 nm – Zr underlayer

According to the XPS theory [10] the XPS integral intensities of the top (I_0) and bottom (I_s) layer for the planar growth are described by:

$$I_0 = I_0^{\infty}\left(1 - e^{-d_0/L}\right), \qquad I_s = I_s^{\infty} e^{-d_0/L}, \tag{1}$$

where: d_0 and L denote the overlayer thickness and escape depth of the excited photoelectrons, respectively.

After transformations of Eq. (1), the ideal planar growth of a bilayer system with perfectly sharp interface is represented by a linear equation:

$$\ln\left[\left(I_s + I_0\right)/I_s\right] = d_0/L \tag{2}$$

The perfectly planar growth of the model bilayer system [10] is represented by the bold solid line in Fig. 4. On the other hand, the model island growth is denoted by the bold broken line [10]. Our experimental results (squares and circles) can be also fitted by a linear regressions (thin broken lines in Fig. 4) but with a significantly lower slope compared to that expected for the ideal planar growth (bold solid line in Fig. 4).

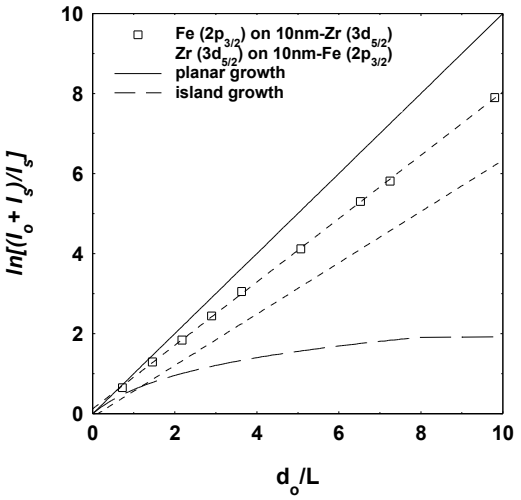

Fig. 4. $\ln[(I_S + I_0)/I_S]$ as a function of d_0/L (see text). Bold solid and broken lines denote theoretical (without interface mixing) planar and island growth of the overlayer [7], respectively. Thin broken lines represent linear fit to the experimental data (squares and circles).

For the calculation of the d_0/L ratio we have taken escape depth values of $L_{\text{Fe-}2p} = 1.15$ nm and $L_{\text{Zr-}3d} = 1.67$ nm [10]. The reason for the significantly lower slope of the experimental data shown in Fig. 4 is the alloying effect at the interface during the deposition process of the bilayers. Magnetisation studies showed that the interface Fe-Zr alloy thickness depends also on the Zr sublayer thickness. We have estimated a minimal interface Fe-Zr alloy thickness as about 2 nm [11]. The interface alloy layer thickness depends on the deposition order and is greater for Zr overlayer deposition on 10 nm – Fe underlayer. However, from the exponential variation of the XPS Fe-2*p* and Zr-3*d* integral intensities with increasing layer thickness we conclude that the Fe and Zr sublayers grow homogeneously [10].

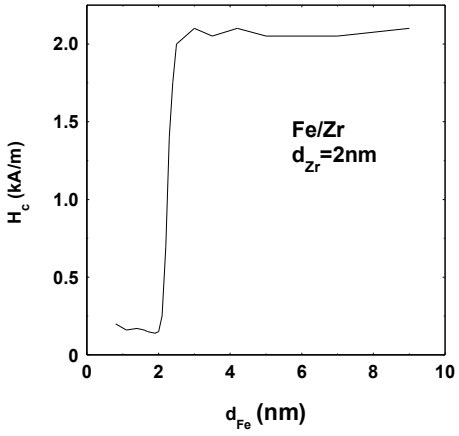

Fig. 5. Coercive field (H_c) as a function of Fe sublayer thickness for wedged Fe/Zr multilayers with d_{Zr}=2 nm

Figure 5 shows H_c values, measured at room temperature, as a function of the Fe sublayer thickness for the wedged Fe/Zr MLs with d_{Zr} = 2 nm. A significant drop of the coercivity with decrease in Fe layer thickness – typically from H_c ~ 2.1-2.3 kA/m to H_c ~ 0.2-0.3 kA/m – can be observed at a critical Fe thickness d_{crit} ~ 2.3 nm. The coercivity behaviour shown in Fig. 5 could be associated with the structural properties of the Fe layer grown onto Zr, similarly to the transition observed earlier for the Co/Zr [2] and Co/Ti [3] MLs. According to above interpretation, iron sublayers grow in the soft magnetic nanocrystalline phase (D << 10 nm) for a thickness lower than the critical one. In that case, the average Fe grain size is significantly smaller than the magnetic exchange length [1] for the iron layer (L_{ex} ~ 15 nm) [1]. For a thickness greater than the d_{crit}, the Fe sublayers undergo a structural transition to the poly-crystalline phase with average in-plane grains size D > 15 nm [1]. Very similar coercivity behaviour to that shown in Fig. 5 has previously been observed for the Co/Ti and Co/Zr MLs [4]. The coercivity transition presented in Fig. 5 was observed only for a Zr sublayer thickness greater than d_{Zr} ~ 0.6 nm. The above effect could be explained by the existence of a minimum Zr sublayer thickness (~ 0.6 nm), which is required for the nanocrystalline growth of Fe, and/or formation of quasi-continuous non-magnetic Zr-Fe layers and a corresponding change of the exchange energy between the Fe sublayers.

For the Fe/Zr MLs with polycrystalline Fe sublayers (d_{Fe} > 2.3 nm) we have observed a small in-plane, highly dispersed uniaxial anisotropy (H_k ~ 1-2 kA/m). The MLs with nano-crystalline Fe sublayers (d_{Fe} < 2.3 nm) showed a well-defined in-plane uniaxial anisotropy (H_k ~ 2-4 kA/m). The origin of the uniaxial anisotropy in the Fe/Zr MLs could be associated with Fe grain deformation during the deposition process. In our case the Fe source is mounted at an angle of about 20° from the normal to the substrate. Such a sputtering configuration could induce deformation of the deposited Fe grains in a preferred direction in such a way that the easy axis of the uniaxial anisotropy is placed along the grains.

4. CONCLUSION

The planar growth of the Fe and Zr sublayers was confirmed *in-situ* by X-ray photoelectron spectroscopy. Iron sublayers grow on sufficiently thick zirconium sublayer in the soft magnetic nanocrystalline phase up to a critical thickness $d_{crit} \sim 2.3$ nm. For a thickness greater than d_{crit}, the Fe sublayers undergo a structural transition to the polycrystalline phase with much higher coercivity.

Acknowledgements

This work was financially supported by the Polish Committee for Scientific Research under grant No. PBZ KBN 044/P03/02 JB.

References

[1] G. Herzer, J. Magn. Magn. Mater. **157/158**, 133 (1996).
[2] L. Smardz, K. Le Dang, H. Niedoba, and K. Chrzumnicka, J. Magn. Magn. Mater. **140-144**, 569 (1995).
[3] L. Smardz, Sol. State Comm. **112**, 693 (1999).
[4] L. Smardz, K. Smardz, and R. Czajka, Cryst. Res. Technol. **36**, 1019 (2001).
[5] L. Smardz, H. Niedoba, B. Mirecki, F. Stobiecki, and B. Szymański, J. Magn. Magn. Mater. **140-144**, 1899 (1995).
[6] L. Smardz, Czech. J. Phys. **52**, 209 (2002).
[7] K. Samwer, Phys. Reports **161**, 3 (1988).
[8] F. J. Castaňo, T. Stobiecki, M. R. J. Gibbs, M. Czapkiewicz, J. Wrona, and M. Kopcewicz, Thin Sol. Films **348**, 233 (1999).
[9] T. Stobiecki, M. Kopcewicz, and F. J. Castaňo, Chaos, Solitons & Fractals **10**, 2031 (1999).
[10] D. Briggs, in: *Handbook of X-ray and ultraviolet photoelectron spectroscopy*, ed. D. Briggs (Heyden & Son Ltd., London – Philadelphia – Rheine, 1977) p. 153.
[11] L. Smardz, to be published.